

Wavepacket interference of two photons through a beam splitter: from temporal entanglement to wavepacket shaping

Zhaohua Tian,¹ Qi Liu,^{1,2} Yu Tian,^{1,2} and Ying Gu^{1,2,3,4,5,*}

¹*State Key Laboratory for Mesoscopic Physics, Department of Physics, Peking University Beijing 100871, China.*

²*Frontiers Science Center for Nano-optoelectronics & Collaborative Innovation Center of Quantum Matter & Beijing Academy of Quantum Information Sciences, Peking University, Beijing 100871, China*

³*Collaborative Innovation Center of Extreme Optics, Shanxi University, Taiyuan, Shanxi 030006, China*

⁴*Peking University Yangtze Delta Institute of Optoelectronics, Nantong 226010, China*

⁵*Hefei National Laboratory, Hefei 230088, China*

(Dated: May 8, 2024)

Quantum interferences based on beam splitting are widely used for entanglement. However, the quantitative description of the entanglement and wavepacket shaping facilitated by this entanglement remain unexplored. Here we analytically study the interference of two photons with different temporal shapes through a beam splitter (BS), then propose its application in temporal entanglement and shaping of photons. The temporal entanglement described by Von Neumann entropy is determined by the splitting ratio of BS and temporal indistinguishability of input photons. Maximum entanglement can be achieved with a 50/50 BS configuration. Then, detecting one of the entangled photons at a specific time enables the probabilistic shaping of the other photon. This process can shape the exponentially decaying (ED) wavepacket into the ED sine shapes, which can be further shaped into Gaussian shapes with fidelity exceeding 99%. The temporal entanglement and shaping of photons based on interference may solve the shape mismatch issues in large-scale optical quantum networks.

I. INTRODUCTION

The non-classical interference processes among photons based on beam splitting are essential for both fundamental physics [1] and applications in quantum information processing [2, 3]. Present studies on quantum interference primarily concentrate on identical photons, while the fruitful information on partially indistinguishable photons with different temporal shapes, has not been fully recognized. Over the past decades, researchers

have demonstrated that temporal entanglement can be realized through the wavepacket interference of photons [4–7]. Based on time-resolved measurements, quantum beat patterns on correlation functions have been theoretically predicted [8, 9] and experimentally demonstrated [10, 11]. However, until now, a comprehensive and quantitative description of the temporal entanglement generated through wavepacket interference is lacking. Furthermore, the modulation of the entanglement and the utilization of this entanglement as a quantum resource in optical quantum information processes remain elusive.

The temporal shape of photons also plays a crucial

* ygu@pku.edu.cn

role in the light-matter interactions [12–15], deterministic quantum state transfer [16] and implementation of quantum logic gates [17, 18]. Therefore, shaping the wavepacket of photons on demand has emerged as a pivotal aspect of quantum photonics. Current methods for shaping the photons include manipulating the emission of the quantum emitters dynamically [16] or passively [19], direct phase modulation [20, 21], spectral filtering [22], and manipulating one of the entangled photon pairs [23, 24]. Nevertheless, the temporal shaping based on entanglement generated from photon wavepacket interference via beam splitting remains unexplored.

In this research, we study the interference of two photon wavepackets with different temporal shapes through a beam splitter (BS). The two initially temporally separable photons become entangled after passing through the BS. Employing Schmidt decomposition approach to analyze the entanglement entropy, the measure of entanglement for output state are obtained. The entanglement degree is determined by the photon temporal indistinguishability and splitting ratio of BS. By utilizing this entanglement and detecting one of the entangled photons at a specific time, temporal shaping of the other photon can be probabilistically achieved in a heralded way. There are two exact examples: (1) the exponentially decaying (ED) wavepacket can be shaped into the ED sine shapes and (2) the ED sine can be further shaped into Gaussian shapes with fidelity higher than 99%. The temporal entanglement and shaping of photons based on interference may address the shape mismatch issues in complex large-scale optical quantum networks.

The paper is organized as follows. In Sec. II, we give the analytical expression of the output state. A quantitative and comprehensive description of the temporal entanglement of the output state is given in Sec.

III. Then the photon temporal shaping scheme based on beam splitting and two exact examples are demonstrated in IV. Finally, we conclude in Sec. V.

II. ANALYTICAL EXPRESSION OF THE OUTPUT STATE

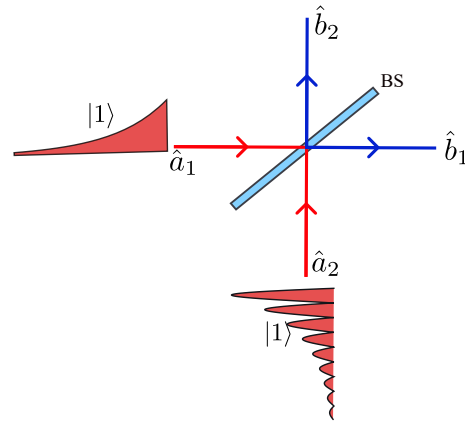


FIG. 1. Schematic for the wavepacket interference of two photons through a beam splitter.

As shown in Fig. 1, we consider the interference of two photons with different temporal shapes through a two-port BS. The input state is a two-mode Fock state

$$|\psi_{\text{in}}\rangle = \int f_1(\tau_1) \hat{a}_1^\dagger(\tau_1) d\tau_1 \int f_2(\tau_2) \hat{a}_2^\dagger(\tau_2) d\tau_2 |0, 0\rangle, \quad (1)$$

where $f_n(\tau_n)$ is the temporal shape of the single photon wavepacket in the n -th input port of BS and satisfies the normalization condition $\int |f_n(\tau)|^2 d\tau = 1$, and $\hat{a}_n^\dagger(\tau)$ ($\hat{a}_n(\tau)$) is the continuous time creation (annihilation) operator [25]. The linear relationship between the operators in the input and output ports (denoted by $\hat{b}_n(\tau)$) can be described by the scattering matrix $\begin{pmatrix} \hat{b}_1(\tau) \\ \hat{b}_2(\tau) \end{pmatrix} = \begin{pmatrix} t & r \\ -r & t \end{pmatrix} \begin{pmatrix} \hat{a}_1(\tau) \\ \hat{a}_2(\tau) \end{pmatrix}$, where t, r are the transmission and reflection coefficients of BS. The commutation relations of these continuous mode operators are $[\hat{a}_n(\tau_1), \hat{a}_n^\dagger(\tau_2)] = \delta(\tau_1 - \tau_2)$, $[\hat{b}_n(\tau_1), \hat{b}_n^\dagger(\tau_2)] =$

$\delta(\tau_1 - \tau_2)$. For convenience, we set t and r to be real numbers. For a lossless BS, $t^2 + r^2 = 1$.

After passing through the BS, the output state could be expressed as

$$|\psi_{\text{out}}\rangle = \sqrt{P_{0,2}}|0, 2\rangle + \sqrt{P_{1,1}}|1, 1\rangle + \sqrt{P_{2,0}}|2, 0\rangle, \quad (2)$$

$P_{m,2-m}$ denotes the probabilities of different outcomes, which can be expressed as

$$P_{2,0} = P_{0,2} = t^2 r^2 (1 + |J|^2), \quad (3a)$$

$$P_{1,1} = t^4 + r^4 - 2t^2 r^2 |J|^2, \quad (3b)$$

where $J = \int f_1(\tau) f_2^*(\tau) d\tau$ is the temporal indistinguishability factor between the two input photons and $0 \leq |J| \leq 1$. $|J| = 1$ indicates perfect photon indistinguishability and $|J| = 0$ means the two photons are completely distinguishable. Therefore, the probability of each outcome is solely determined by the photon indistinguishability factor and splitting ratio of BS. The components $|0, 2\rangle, |1, 1\rangle, |2, 0\rangle$ are expressed as follows

$$|0, 2\rangle \equiv \iint F_{0,2}(\tau_1, \tau_2) \frac{\hat{b}_2^\dagger(\tau_1) \hat{b}_2^\dagger(\tau_2)}{\sqrt{2}} d\tau_1 d\tau_2 |0, 0\rangle, \quad (4a)$$

$$|1, 1\rangle \equiv \iint F_{1,1}(\tau_1, \tau_2) \hat{b}_1^\dagger(\tau_1) \hat{b}_2^\dagger(\tau_2) d\tau_1 d\tau_2 |0, 0\rangle, \quad (4b)$$

$$|2, 0\rangle \equiv \iint F_{2,0}(\tau_1, \tau_2) \frac{\hat{b}_1^\dagger(\tau_1) \hat{b}_1^\dagger(\tau_2)}{\sqrt{2}} d\tau_1 d\tau_2 |0, 0\rangle, \quad (4c)$$

where $F_{2,0}(\tau_1, \tau_2) = -F_{0,2}(\tau_1, \tau_2) = rt[f_1(\tau_1) f_2(\tau_2) + f_2(\tau_1) f_1(\tau_2)]/\sqrt{P_{2,0}}$, and $F_{1,1}(\tau_1, \tau_2) = [t^2 f_1(\tau_1) f_2(\tau_2) - r^2 f_2(\tau_1) f_1(\tau_2)]/\sqrt{P_{1,1}}$. Here $F_{m,2-m}(\tau_1, \tau_2)$ denotes the temporal shape or wavefunction of the component $|m, 2-m\rangle$, normalized by $\iint |F_{m,2-m}(\tau_1, \tau_2)|^2 d\tau_1 d\tau_2 = 1$. Therefore, after passing through the BS, the wavefunction of different components of the output state includes the coherent superposition of the product of temporal shapes $f_n(\tau)$,

whose inseparable suggests the presence of entanglement. The information of the temporal entanglement is embedded within the analytical expressions of the wavefunction, which will be explored in depth in the following section.

III. TEMPORAL ENTANGLEMENT OF THE OUTPUT STATE

It can be seen from Eq. (4) that the wavefunction of the output state components $|2, 0\rangle, |1, 1\rangle$, and $|0, 2\rangle$ is inseparable, revealing that the two photons are entangled temporally. This implies that temporal entanglement can be generated through the wavepacket interference of two photons with different temporal shapes. Prior studies have primarily concentrated on measuring the joint spectral density (JSD) profile [9–11, 26, 27], specifically focusing on the entanglement of the outcome $|1, 1\rangle$. Here we give a comprehensive and quantitative examination of the entanglement across all three outcomes $|2, 0\rangle, |1, 1\rangle$, and $|0, 2\rangle$.

First, we present the analytical expression for quantifying the entanglement of each component of the output state. We employ the Von Neumann entropy $\mathcal{S}_{|m,2-m\rangle}$ as an exact measure of entanglement, which can be expressed in terms of Schmidt coefficients as

$$\begin{aligned} \mathcal{S}_{|1,1\rangle} &= - \sum_{n=\pm} |\lambda_n^1|^2 \log_1 |\lambda_n^1|^2, \\ \mathcal{S}_{|2,0\rangle} &= \mathcal{S}_{|0,2\rangle} = - \sum_{n=\pm} |\lambda_n^2|^2 \log_2 |\lambda_n^2|^2. \end{aligned} \quad (5)$$

The Schmidt coefficients λ_n^m satisfy the normalization condition $\sum_{n=\pm} |\lambda_n^m|^2 = 1$ and are obtained by performing Schmidt decomposition on the wavefunction of the output state components (See Appendix A). The analytical expressions of Schmidt coefficients λ_n^m are

$$|\lambda_{\pm}^1|^2 = \frac{\left[\mathcal{P}^2 + \frac{1}{2}\mathcal{J}^2(1 - \mathcal{P}^2) \pm \mathcal{P}\sqrt{|J|^2\mathcal{J}^2(\mathcal{P} - 1)^2 + (\mathcal{P} - \mathcal{J}^2(\mathcal{P} - 1))^2} \right]}{2(\mathcal{P}^2 + \frac{1}{2}\mathcal{J}^2(1 - \mathcal{P}^2))}, \quad (6a)$$

$$|\lambda_{\pm}^2|^2 = \frac{(1 \pm |J|)^2}{2(1 + |J|^2)}, \quad (6b)$$

where $\mathcal{J} = \sqrt{1 - |J|^2}$, and $\mathcal{P} = t^2 - r^2$ is defined to characterize the photon pathways indistinguishability. If $|\mathcal{P}| = 1$, then $t^2 = 1$ or $t^2 = 0$, the photon pathways are completely distinguishable. Perfect indistinguishable photon pathways need $\mathcal{P} = 0$ which means that $t^2 = r^2 = 1/2$. The Von Neumann entropy \mathcal{S} is in the range $0 \leq \mathcal{S} \leq 1$. $\mathcal{S} > 0$ indicates the two photons are entangled and $\mathcal{S} = 0$ means quantum state is separable. The maximum entanglement $\mathcal{S} = 1$ is achieved when the two Schmidt mode coefficients are equal $|\lambda_+^m|^2 = |\lambda_-^m|^2$, signifying the realization of the two-photon Bell state encoded in the temporal mode. The correctness of the analytical results for the Schmidt decomposition presented above has been verified through numerical methods (Refer to Appendix B for details). According to Eqs. (5) and (6), the entanglement of the output state is solely determined by the photon temporal indistinguishability J and the transmission ratio t^2 of the BS. Additionally, the entanglement of different components varies: the entanglement of the components $|2, 0\rangle$ and $|0, 2\rangle$ are equal which are only related to the photon temporal indistinguishability J , but the entanglement of the component $|1, 1\rangle$ is determined by both the photon indistinguishability and the splitting ratio of BS.

We then systematically investigate the effect of photon indistinguishability $|J|$ and transmission t^2 of BS on the Von Neumann entropies. As depicted in Figs. 2(a) and (b), a common feature is that an increase in the photon

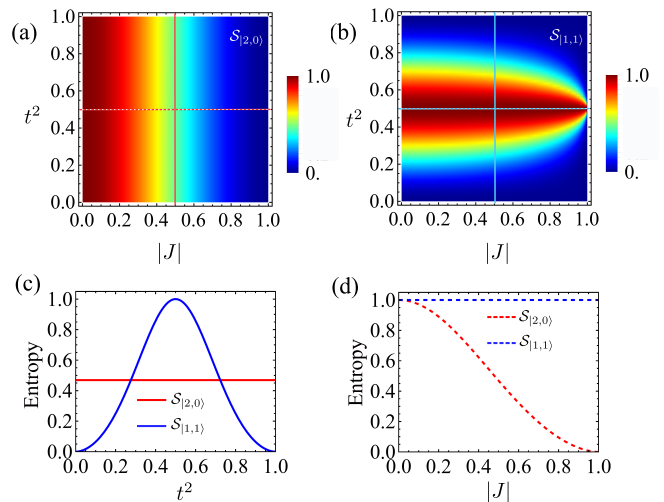


FIG. 2. Von Neumann entropy of the output state for the outcome (a) $|2, 0\rangle$ and (b) $|1, 1\rangle$ as a function of photon indistinguishability and transmission of BS; Slice of the Von Neumann entropy of the outcome $|1, 1\rangle$ (blue line) and $|2, 0\rangle$ (red line) (c) as a function transmission of BS (solid line) when $|J| = 0.5$ and (d) as a function photon indistinguishability (dashed line) when $t^2 = 0.5$.

indistinguishability $|J|$ leads to a decrease in the temporal entanglement for both $|1, 1\rangle$ and $|2, 0\rangle$, except for the case where $t^2 = 0.5$. Maximal entanglement is achieved for $|J| = 0$, i.e., the two input photons are completely distinguishable. In the conventional HOM interference, a perfect NOON state can only be generated when the two photons are completely indistinguishable [1], while our quantitative results show that when examining entanglement within the temporal continuum, entanglement can only be generated when the two interfering photons are partly distinguishable. Furthermore, as illustrated in Fig. 2 (c), the entanglement of $|1, 1\rangle$ can be modulated by adjusting the beam splitting ratio of BS. The max-

imal entanglement is achieved when $t^2 = 0.5$ ($\mathcal{P} = 0$), i.e., the photon pathways are completely indistinguishable. Conversely, the entanglement is zero when $t^2 = 1$ or 0 ($|\mathcal{P}| = 1$), revealing that completely distinguishable photon pathways result in no entanglement for the outcome $|1, 1\rangle$. These quantitative results can serve as valuable guidance for manipulating temporal entanglement generated through interference.

We also discover an intriguing result: the temporal entanglement of component $|1, 1\rangle$ always remains maximal with a 50/50 BS configuration, independent of photon indistinguishability. As depicted in Fig. 2 (d), when $t^2 = 0.5$, as the increase of the photon temporal indistinguishability $|J|$, the entanglement of $|1, 1\rangle$ consistently remains at 1. In this case, it can be proven that, excepting for perfect indistinguishable photons ($|J| = 1$ so that $P_{1,1} = 0$), regardless of the exact form of the two input photons, the component $|1, 1\rangle$ can always be considered as a Bell state encoded in the temporal Schmidt modes $|\phi_{\pm}^1\rangle$ (See Appendix C)

$$|1, 1\rangle = \frac{1}{\sqrt{2}}(|\phi_+^1\rangle_{\hat{b}_1} |\phi_-^1\rangle_{\hat{b}_2} - |\phi_-^1\rangle_{\hat{b}_1} |\phi_+^1\rangle_{\hat{b}_2}), \quad (7)$$

then $|\lambda_-^1|^2 = |\lambda_+^1|^2 = 1/2$ and $\mathcal{S}_{|1,1\rangle} = 1$. The specific form of the input photons $f_n(\tau)$ determines the shapes of the Schmitt modes $\phi_{\pm}^1(\tau)$ but does not change the superposition coefficients between them. This is because the outcome $|1, 1\rangle$ arises from two indistinguishable photon pathways: two photons are either simultaneously reflected or transmitted by the BS. When $t^2 = 0.5$, then $\mathcal{P} = 0$, the two photon pathways are completely indistinguishable. This facilitates the creation of maximized entangled Bell state, the entanglement of which does not depend on specific temporal shapes. When $t^2 \neq 0.5$, the two photon pathways are not completely indistin-

guishable, resulting in a non-maximally entangled state. Consequently, the entanglement is influenced by the indistinguishability of the input photons.

The quantitative results above provide us with a more profound understanding of the mechanism and properties of temporal entanglement generated through wavepacket interference of two photons. This temporal entanglement, as a significant quantum resource, holds potential applications in fundamental physics tests and quantum information processing. In the following section, we will demonstrate its application in temporal shaping of photons.

IV. SINGLE-PHOTON TEMPORAL SHAPING BASED ON TIME-RESOLVED MEASUREMENT

In this section, we will demonstrate that temporal entanglement generated through wavepacket interference of two photons can be utilized for shaping. For temporally entangled photon pairs, shaping one photon can be achieved by manipulating or measuring the other photon. Firstly, we present the relationship between the temporal shapes of the wave packets before and after shaping. Subsequently, we provide two specific examples of wavepacket shaping based on this relationship.

We first present the shaping principle based on wavepacket interference and time-resolved measurement. As depicted in Fig. 3(a) (or Fig. 3(e)), two photon wavepackets with different temporal shapes impinge on the BS and a photon-number-resolved detector (PNRD) is placed at the output port 1 of BS. By detecting only one photon at a specific time t_{dec} , the component $|1, 1\rangle$ can be selected probabilistically. The resulting single photon state in output port 2 can be expressed as

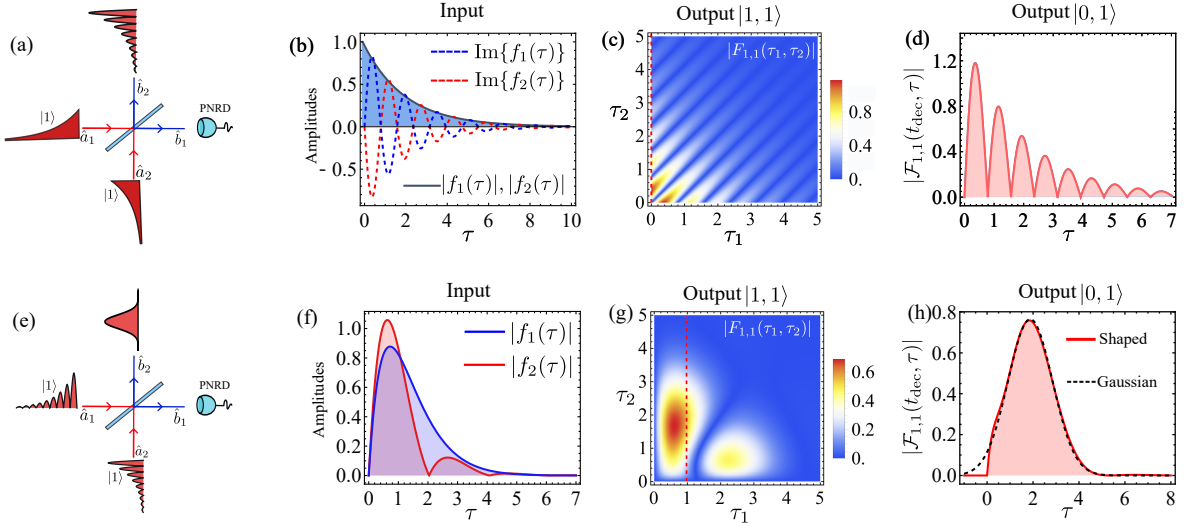


FIG. 3. The temporal shaping scheme and examples. (a)-(d) Single photon with ED sine shape generated via the interference of two ED shaped photons. (e)-(h) Single photon with Gaussian shape generated via the interference of two ED sine shaped photons. The detailed parameters are in the main text. (a), (e) Schematic for single photon temporal shaping based on the interference of two photon wavepackets and time-resolved measurement. A photon-number-resolved detector (PNRD) is placed at the output port 1 of BS. (b), (f) The temporal shapes of the two input photons. (c), (g) The temporal shape of the component $|1, 1\rangle$. The red dashed line denotes the required detection time instant. (d), (h) The temporal shape of resulting single photon state $|0, 1\rangle$ in output port 2 after time-resolved detection.

A. Example: Shaping photon from ED shape into ED sine shape

$$|0, 1\rangle = \int \mathcal{F}_{1,1}(t_{\text{dec}}, \tau) \hat{b}_2^\dagger(\tau) d\tau |0, 0\rangle, \quad (8)$$

with $\mathcal{F}_{1,1}(t_{\text{dec}}, \tau)$ denotes the resulting temporal shape after detection

$$\mathcal{F}_{1,1}(t_{\text{dec}}, \tau) = \frac{1}{\sqrt{\text{nor}}} (t^2 f_1(t_{\text{dec}}) f_2(\tau) - r^2 f_2(t_{\text{dec}}) f_1(\tau)). \quad (9)$$

Here the normalization coefficient, $\text{nor} = \int |\mathcal{F}_{1,1}(t_{\text{dec}}, \tau)|^2 d\tau$, ensures the proper normalization of the state. The shape of the heralded single photon $\mathcal{F}_{1,1}(t_{\text{dec}}, \tau)$ in output port 2 depends on the temporal shapes of two input photons, the transmission of BS, and the time-resolved measurement outcome at a time instant t_{dec} . The joint control of these parameters tailors the temporal shape.

We now demonstrate shaping photon from ED shape into ED sine shape. As shown in 3(a), two detuned ED shaped photons are incident on the entrance ports of a 50/50 BS. By detecting only a single photon at a desired time instant via a PNRD at output port 1 of the BS, single photons with an ED sine shape can be generated at output port 2. The temporal shapes of the two input photons can be expressed as $f_1(\tau) = \sqrt{\Gamma} e^{-i(\Delta\omega - i\Gamma)\tau/2}$, $f_2(\tau) = \sqrt{\Gamma} e^{-i(-\Delta\omega - i\Gamma)\tau/2}$, here $\Gamma, \Delta\omega$ denote the spectral width and detuning of two input photons, respectively. Following Eq. (4), the wavefunction of the component $|1, 1\rangle$ after passing the symmetric BS is $F_{1,1}(\tau_1, \tau_2) = i\sqrt{\frac{1}{P_{1,1}}} e^{-\Gamma(\tau_1 + \tau_2)/2} \sin(\Delta\omega(\tau_2 - \tau_1)/2)$. By detecting only one photon at time instant $t_{\text{dec}} = 0$ at output port 1 of BS, the temporal shape of the resulting

single photon at output port 2 is

$$\mathcal{F}_{1,1}(0, \tau) = i\sqrt{\frac{\Gamma(\Delta\omega^2 + \Gamma^2)}{\Delta\omega^2/2}} e^{-\Gamma\tau/2} \sin(\Delta\omega\tau/2), \quad (10)$$

which is the required ED sine shape.

We offer a more intuitive demonstration of the shaping process described above with specific parameters. The temporal shapes of two input wavepackets with ED shapes are shown in Fig. 3 (b). The linewidth of the two photons are the same $\Gamma = 1$ and the detuning is set to be $\Delta\omega = 8$. After passing through the BS, the wavefunction of the component $|1, 1\rangle$ is depicted in Fig. 3 (c), where quantum beat pattern can be observed. By detecting only one photon at time instant $t_{\text{dec}} = 0$ at output port 1 of BS, as indicated by the red dashed lines in Fig. 3(c), the resulting single photon at port 2 with required ED shape is shown in Fig. 3(d).

B. Example: Shaping photon from ED sine shape into Gaussian shape

We further demonstrate shaping photon from ED sine shape into Gaussian shape, which is crucial for achieving high-fidelity deterministic optical quantum storage [16] and optical quantum logic gates [17, 28]. As shown in Fig. 2(e), two photons with different ED sine shapes impinge on the entrance ports of a BS. The temporal shape of the input photons can be described as $f_n(\tau) = \sqrt{\frac{\Gamma_n(4\omega_n^2 + \Gamma_n^2)}{2\omega_n^2}} e^{-\Gamma_n\tau/2} \sin(\omega_n\tau)$, where Γ_n and ω_n represent the spectral width and resonant frequency, respectively. The Gaussian shape can be expressed as $f_{\text{Gau}}(\tau) = \sqrt{\frac{\Gamma_{\text{Gau}}}{\sqrt{\pi}}} e^{-\frac{1}{2}(\tau-\tau_0)^2\Gamma_{\text{Gau}}^2}$, where Γ_{Gau} and τ_0 denote the spectral width and the delay time of photon wavepacket, respectively. We aim for excellent indistinguishability between the interferometrically synthesized

wavepacket and the Gaussian shape wavepacket. This translates into realizing the following optimization problem:

$$\text{Maximize: } F_{\text{shaping}}(x) = \left| \int f_{\text{Gau}}^*(\tau) \mathcal{F}_{1,1}(t_{\text{dec}}, \tau) d\tau \right|^2, \quad (11)$$

here F_{shaping} represents the shaping fidelity, defined as the square of the indistinguishability between the interferometrically synthesized wavepacket and the Gaussian wavepacket. In optimization, the linewidth of the Gaussian shape Γ_{Gau} is fixed, and the parameters to be optimized are $x = \{\Gamma_1, \Gamma_2, \omega_1, \omega_2, t, \tau_0, t_{\text{dec}}\}$, including the linewidth of the input photons Γ_n , resonant frequency ω_n , transmission coefficients t of BS, delay time of the shaped Gaussian shape τ_0 and an appropriate detection time t_{dec} .

Now, we intuitively demonstrate the process of obtaining high-fidelity Gaussian-shaped photons through shaping. We set the linewidth of the target Gaussian-shaped photons to be $\Gamma_{\text{Gau}} = 1$. After optimization, the optimal parameters are $x = \{2.04, 2.60, -1.49, 0.380, 0.768, 1.81, 0.940\}$. The corresponding temporal shapes of the two input photons are shown in Fig. 3(f), both of which are ED sine shapes with different linewidths and resonant frequencies. The wavefunction of $|1, 1\rangle$ after passing through the BS is shown in Fig. 3(g). We can observe that the output wavefunction is entangled temporally. By detecting only one photon at output port 1 of BS at time $t_{\text{dec}} = 0.940$, as indicated by the red dashed lines in Fig. 3(g), the resulting single photon temporal shape at output port 2 of BS is drawn in Fig. 3(h). The target Gaussian shape is also shown in Fig. 3(h) as a reference. We can observe that the temporal shape generated through interference is very similar to the target Gaussian shape. The corresponding shap-

ing fidelity is 0.996. Compared to the shaping methods demonstrated in the Refs [23, 24], our approach achieves high-fidelity Gaussian-shaped photons without the need for nonlinear process.

We briefly discuss the influence of time resolution of the detector on the shaping. In the above two examples, we have assumed that detectors could precisely detect photons at specific moments t_{dec} . However, in actual detection processes, the resolution of detectors is always limited. We can only confirm the detection of photons within a certain time interval $(t_{\text{dec}} - t_{\text{R}}/2, t_{\text{dec}} + t_{\text{R}}/2)$, where t_{R} denotes the detection time resolution of the detector. The effects of detection time resolution t_{R} on probability and fidelity of shaping are demonstrated in Appendix C. The limited resolved time of detectors could increase the success probability but decrease the fidelity of shaping. A trade-off between requirements of probability and fidelity should be considered in experiments.

The temporal shaping scheme discussed above provides new insights into wavepacket transformation in quantum information processing. Shaping photons on demand at various stages of optical quantum information processing is crucial. Failure to do so may result in temporal shape mismatch issues, which can affect photon interference and light-matter interactions, thereby further impacting the corresponding quantum information processes. In the two examples we have presented the conversion of commonly encountered single photon temporal shapes can be achieved, offering a solution to mitigate the impact of temporal shape mismatch issues in complex large-scale optical quantum networks. In principle, based on the wavepacket interference of two photons, more temporal shaping functionalities can be realized, thereby facilitating the adaptation to various task requirements in quantum information.

V. SUMMARY

In summary, we have studied the interference of two photon wavepackets with different temporal shapes through BS. We have employed the Von Neumann entropy to quantitatively describe the entanglement of the output state and found analytically that the entanglement is directly determined by the temporal indistinguishability of photons and the splitting ratio of BS. Maximum entanglement for the outcome $|1, 1\rangle$ can be achieved with a 50/50 BS configuration, while completely distinguishable input photons will maximize the entanglement of the outcomes $|2, 0\rangle$ and $|0, 2\rangle$. We have further demonstrated that the temporal shaping of a single photon can be achieved probabilistically by detecting one of the entangled photons. Our work reveals the crucial roles of photon temporal and photon pathway indistinguishability in the generation of temporal entanglement. The proposed scheme of single-photon temporal shaping also offers a solution to the issues of shape mismatch in complex large-scale optical quantum networks.

ACKNOWLEDGMENTS

This work was supported by the National Natural Science Foundation of China (11974032), Key R&D Program of Guangdong Province (2018B030329001) and the Innovation Program for Quantum Science and Technology (2021ZD0301500).

Appendix A: Schmidt decomposition of the output state

By performing the Schmidt decomposition on different components of the output state, the wavefunction $F_{m,2-m}(\tau_1, \tau_2)$ will be ultimately expressed as a weighted

sum of products of two adjoint function bases $\{\phi_n^m\}$ and $\{\tilde{\phi}_n^m\}$,

$$F_{m,2-m}(\tau_1, \tau_2) = \sum_{n=1}^N \lambda_n^m \phi_n^m(\tau_1) \tilde{\phi}_n^m(\tau_2), \quad (\text{A1})$$

where N denotes the number of Schmidt modes. The decomposition coefficients satisfy the normalization condition $\sum_n^N |\lambda_n^m|^2 = 1$. The Schmidt-mode single photon wavefunctions $\phi_n^m(\tau), \tilde{\phi}_n^m(\tau)$ form a complete set of orthogonal functions $\int \phi_i^{m*}(\tau) \phi_j^m(\tau) d\tau = \delta_{i,j}, \int \tilde{\phi}_i^{m*}(\tau) \tilde{\phi}_j^m(\tau) d\tau = \delta_{i,j}$. Following the standard procedure [29], the temporal correlation function $K_m(\tau_1, \tau_2), \tilde{K}_m(\tau_1, \tau_2)$ of the wavefunction $F_{m,2-m}(\tau_1, \tau_2)$ should be first obtained

$$K_m(\tau_1, \tau_2) = \int F_{m,2-m}(\tau_1, \tau) F_{2-m}^*(\tau_2, \tau) d\tau, \quad (\text{A2a})$$

$$\tilde{K}_m(\tau_1, \tau_2) = \int F_{m,2-m}(\tau, \tau_1) F_{2-m}^*(\tau, \tau_2) d\tau, \quad (\text{A2b})$$

then the Schmidt modes $\phi_n^m(\tau), \tilde{\phi}_n^m(\tau)$ and coefficients $|\lambda_n^m|^2$ are solutions of the following integral eigenvalue

$$F_{2,0}(\tau_1, \tau_2) = \frac{1}{\sqrt{2P_{2,0}}} [\mathcal{J}\xi_1(\tau_1)\xi_2(\tau_2) + \mathcal{J}\xi_2(\tau_1)\xi_1(\tau_2) + 2J^*\xi_1(\tau_1)\xi_1(\tau_2)], \quad (\text{A5a})$$

$$F_{0,2}(\tau_1, \tau_2) = -\frac{1}{\sqrt{2P_{0,2}}} [\mathcal{J}\xi_1(\tau_1)\xi_2(\tau_2) + \mathcal{J}\xi_2(\tau_1)\xi_1(\tau_2) + 2J^*\xi_1(\tau_1)\xi_1(\tau_2)], \quad (\text{A5b})$$

$$F_{1,1}(\tau_1, \tau_2) = \frac{1}{\sqrt{P_{1,1}}} [\mathcal{J}T\xi_1(\tau_1)\xi_2(\tau_2) - \mathcal{J}R\xi_2(\tau_1)\xi_1(\tau_2) + \mathcal{P}J^*\xi_1(\tau_1)\xi_1(\tau_2)]. \quad (\text{A5c})$$

By inserting the results in Eq. (A5) into Eq. (A2), the temporal correlation functions can be analytically expressed as follows

$$K_m(\tau_1, \tau_2) = \boldsymbol{\xi}^T(\tau_1) \mathbf{M}^m \boldsymbol{\xi}^*(\tau_2), \quad (\text{A6})$$

equations

$$\int K_m(\tau, \tau') \phi_i^m(\tau') d\tau' = |\lambda_i^m|^2 \phi_i^m(\tau), \quad (\text{A3a})$$

$$\int \tilde{K}_m(\tau, \tau') \tilde{\phi}_i^m(\tau') d\tau' = |\lambda_i^m|^2 \tilde{\phi}_i^m(\tau), \quad (\text{A3b})$$

which should be done numerically in general.

To analytically perform the Schmidt decomposition, we first construct the new orthogonal and normalized basis vector $\boldsymbol{\xi}(\tau) = [\xi_1(\tau), \xi_2(\tau)]^T$ via the Gram-Schmidt process based on the wavefunctions $f_n(\tau)$ of input photons

$$\xi_1(\tau) = f_1(\tau), \quad (\text{A4a})$$

$$\xi_2(\tau) = \frac{f_2(\tau) - J^* f_1(\tau)}{\mathcal{J}}. \quad (\text{A4b})$$

This way, the output temporal shapes are the coherent superposition of these orthogonal basis vectors

$$\tilde{K}_m(\tau_1, \tau_2) = \boldsymbol{\xi}^T(\tau_1) \tilde{\mathbf{M}}^m \boldsymbol{\xi}^*(\tau_2), \quad (\text{A7})$$

where $\tilde{\mathbf{M}}^m, \mathbf{M}^m$ are the corresponding coefficient matrix

$$\mathbf{M}^1 = \frac{1}{\sqrt{P_{1,1}}} \begin{pmatrix} \mathcal{P}^2 |J|^2 + T^2 \mathcal{J}^2 & -R\mathcal{J}\mathcal{P}J^* \\ -R\mathcal{J}\mathcal{P}J & R^2 \mathcal{J}^2 \end{pmatrix}, \quad (\text{A8a})$$

$$\tilde{\mathbf{M}}^1 = \frac{1}{\sqrt{P_{1,1}}} \begin{pmatrix} \mathcal{P}^2 |J|^2 + R^2 \mathcal{J}^2 & T\mathcal{J}\mathcal{P}J^* \\ T\mathcal{J}\mathcal{P}J & T^2 \mathcal{J}^2 \end{pmatrix}, \quad (\text{A8b})$$

$$\mathbf{M}^{2/0} = \tilde{\mathbf{M}}_{2/0} = \frac{1}{\sqrt{2(1+|J|^2)}} \begin{pmatrix} 4 - 3\mathcal{J}^2 & 2J^* \mathcal{J} \\ 2J\mathcal{J} & \mathcal{J}^2 \end{pmatrix}, \quad (\text{A8c})$$

and $T = t^2, R = r^2$ are the transmission and reflection ratios of BS. By performing eigendecomposition on the coefficient matrix $\mathbf{M}^m, \tilde{\mathbf{M}}^m$, the correlation functions can be written in a diagonal form

$$\begin{aligned} K_m(\tau_1, \tau_2) &= \boldsymbol{\xi}^T(\tau_1) \mathbf{V}^m \begin{pmatrix} |\lambda_1^m|^2 & 0 \\ 0 & |\lambda_2^m|^2 \end{pmatrix} (\mathbf{V}^m)^{-1} \boldsymbol{\xi}^*(\tau_2) \\ &= \boldsymbol{\phi}^T(\tau_1) \begin{pmatrix} |\lambda_1^m|^2 & 0 \\ 0 & |\lambda_2^m|^2 \end{pmatrix} \boldsymbol{\phi}^*(\tau_2), \end{aligned} \quad (\text{A9})$$

$$\begin{aligned} \tilde{K}_m(\tau_1, \tau_2) &= \tilde{\boldsymbol{\xi}}^T(\tau_1) \tilde{\mathbf{V}}^m \begin{pmatrix} |\lambda_1^m|^2 & 0 \\ 0 & |\lambda_2^m|^2 \end{pmatrix} (\tilde{\mathbf{V}}^m)^{-1} \tilde{\boldsymbol{\xi}}^*(\tau_2) \\ &= \tilde{\boldsymbol{\phi}}^T(\tau_1) \begin{pmatrix} |\lambda_1^m|^2 & 0 \\ 0 & |\lambda_2^m|^2 \end{pmatrix} \tilde{\boldsymbol{\phi}}^*(\tau_2). \end{aligned} \quad (\text{A10})$$

Here the matrices $\mathbf{V}^m = [V_1^m, V_2^m], \tilde{\mathbf{V}}^m = [\tilde{V}_1^m, \tilde{V}_2^m]$ are composed of the eigenvectors of matrices \mathbf{M}^m and $\tilde{\mathbf{M}}^m$, respectively. The eigenvalues of $\mathbf{M}^m, \tilde{\mathbf{M}}^m$ are the corresponding Schmidt coefficients $|\lambda_n^m|^2$. The two Schmidt modes $\{\phi_+^m(\tau), \phi_-^m(\tau)\}$ and $\{\tilde{\phi}_+^m(\tau), \tilde{\phi}_-^m(\tau)\}$ can be constructed via the orthogonal basis vector $\boldsymbol{\xi}(\tau)$ and the

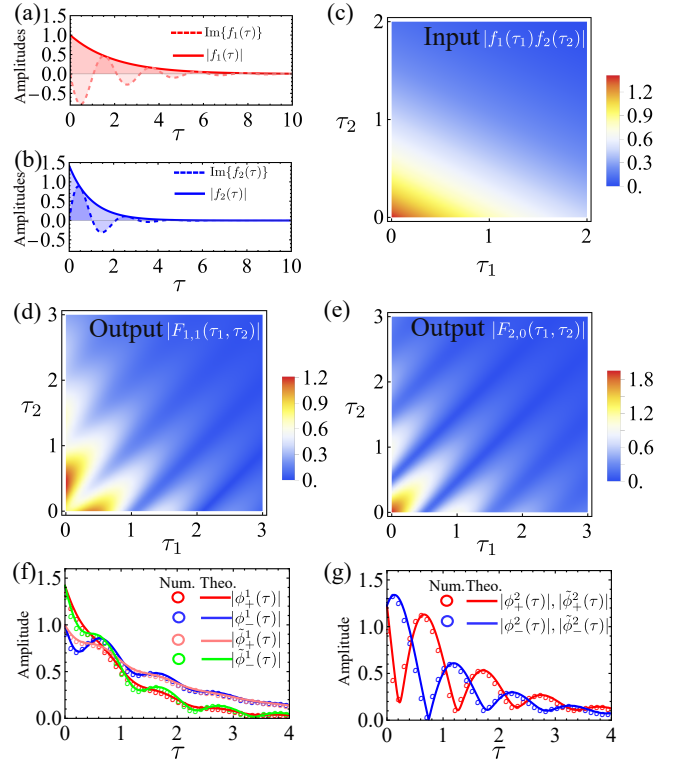


FIG. 4. Example demonstrating the Schmidt decomposition of the output state and numerical validation of the analytical results. The temporal shape of two photon wavepackets input from (a) port 1 and (b) port 2 of BS. The absolute value of (c) the input two-photon wavefunction $|f_1(\tau_1)f_2(\tau_2)|$; The output two-photon wavefunction for the part (d) $|1, 1\rangle$ and (e) $|2, 0\rangle$; Comparison between the Schmidt modes from numerical simulations (circles) and from analytical results (solid curves) for the outcomes (f) $|1, 1\rangle$ and (g) $|2, 0\rangle$. Here we take $\Gamma_1 = 1, \Gamma_2 = 2, \omega_1 = -3, \omega_2 = 3$ and $t^2 = 1/4$.

eigenvectors of matrices $\tilde{\mathbf{M}}^m, \tilde{\mathbf{M}}^m$ as follows

$$\begin{pmatrix} \phi_+^m(\tau) \\ \phi_-^m(\tau) \end{pmatrix} = [\mathbf{V}^m]^T \begin{pmatrix} \xi_1(\tau) \\ \xi_2(\tau) \end{pmatrix}, \quad (\text{A11a})$$

$$\begin{pmatrix} \tilde{\phi}_+^m(\tau) \\ \tilde{\phi}_-^m(\tau) \end{pmatrix} = [\tilde{\mathbf{V}}^m]^T \begin{pmatrix} \xi_1(\tau) \\ \xi_2(\tau) \end{pmatrix}. \quad (\text{A11b})$$

Here $[\mathbf{V}^m]^T, [\tilde{\mathbf{V}}^m]^T$ denote the transpose of matrices $\mathbf{V}^m, \tilde{\mathbf{V}}^m$.

Appendix B: Example of the Schmidt decomposition and numerical validation

As an exact example, we specifically consider the interference of two photons with different ED shapes $f_n(\tau) = \sqrt{\Gamma_n} e^{-i(\omega_n - \frac{i\Gamma_n}{2})\tau}$, where Γ_n, ω_n denote the spectral width, and resonant frequency of photon wavepacket, respectively. Figures 4(a) and (b) show the temporal shapes of the two input photons, respectively. The absolute value is represented by solid curves, and the imaginary value is represented by dashed curves. The two-dimensional distribution of the two-photon wavefunction for the input quantum state is shown in Fig. 4 (c), which shows exponentially decay in both time axis τ_1, τ_2 . From Eq. (4), we know that the wavefunctions of the components $|2, 0\rangle$ and $|0, 2\rangle$ differ only by a sign. Therefore, in the following discussions on wavefunctions, we will primarily focus on the part $|2, 0\rangle$. After passing through the BS, the output two-photon wavefunctions $|F_{1,1}(\tau_1, \tau_2)|$ and $|F_{2,0}(\tau_1, \tau_2)|$ are shown in Figs. 4 (d) and (e), respectively. We can observe that the temporally overlapping parts interfere either destructively or constructively, forming interference fringes. With time-resolved detection, the interference fringes primarily manifest as the quantum beat effects of the second order correlation function [10]. The photon indistinguishability can be obtained by calculating the temporal overlap integral of the two input photons which is $|J| = 0.229$. According to the analytical expression in Eq. (6), the Schmidt coefficients of the part $|2, 0\rangle$ and $|1, 1\rangle$ are $|\lambda_+^2|^2 = 0.283, |\lambda_-^2|^2 = 0.717$, and $|\lambda_+^1|^2 = 0.905, |\lambda_-^1|^2 = 0.095$, respectively, confirming that the output states are entangled.

To verify the correctness of the analytical Schmidt decomposition results, we tackle the eigenvalue problem in Eq. (A3) numerically. We discretize

$K_m(\tau_1, \tau_2), \tilde{K}_m(\tau_1, \tau_2)$ into a 100×100 grid on a square temporal domain ranging from 0 to 10. The corresponding eigenvalues agree well with the analytical results. The Schmidt modes corresponding to outcomes $|1, 1\rangle$ and $|2, 0\rangle$ are depicted in Figs. 4(f) and (g), respectively. For wavefunctions $F_{2,0}(\tau_1, \tau_2)$, due to the permutation symmetry $F_{2,0}(\tau_1, \tau_2) = F_{2,0}(\tau_2, \tau_1)$, this leads to $\phi_+^2(\tau) = \tilde{\phi}_+^2(\tau), \phi_-^2(\tau) = \tilde{\phi}_-^2(\tau)$. We can observe that the temporal shape of Schmidt modes obtained from analytical expression (solid curves) and from numerical simulations (circles) exhibit good agreement.

Appendix C: Schmidt decomposition of $|1, 1\rangle$ for a 50/50 BS

Following the expression in Eq. (A5), for a 50/50 BS, $t^2 = r^2 = 1/2$, then $\mathcal{P} = 0$, the wavefunction $F_{1,1}(\tau_1, \tau_2)$ turns out to be

$$F_{1,1}(\tau_1, \tau_2) = \frac{1}{\sqrt{2}} [\xi_1(\tau_1) \xi_2(\tau_2) - \xi_2(\tau_1) \xi_1(\tau_2)], \quad (\text{C1})$$

which is already a standard form of the Schmidt decomposition, with the Schmidt modes as $\phi_+^1(\tau) = \tilde{\phi}_-^1(\tau) = \xi_1(\tau), \phi_-^1(\tau) = \tilde{\phi}_+^1(\tau) = \xi_2(\tau)$ and the Schmidt coefficients are $\lambda_{\pm}^1 = \pm \frac{1}{\sqrt{2}}$. Therefore, as demonstrated in Eq (7), the component $|1, 1\rangle$ could be written as a Bell state encoded in Schmidt modes $|\phi_{\pm}^1\rangle_{\hat{b}_n} = \int \phi_{\pm}^1(\tau) d\tau \hat{b}_n^\dagger(\tau) |0\rangle$.

Appendix D: Effect of limited resolved time on heralding probability and fidelity

Assuming the time interval that the detector could resolve is t_R , following a successful time-resolved detection at output port 1 of BS, the resulting single photon state at output 2 is

$$|0, 1\rangle = \int_{t_{\text{dec}}-t_R/2}^{t_{\text{dec}}+t_R/2} \int \mathcal{F}_{1,1}(t_{\text{dec}}, \tau) \hat{b}_2^\dagger(\tau) d\tau_1 d\tau_2 |0, 0\rangle. \quad (\text{D1})$$

Here the normalization coefficient becomes to be $\text{nor} = \int_{t_{\text{dec}}-t_R/2}^{t_{\text{dec}}+t_R/2} \int |F_{1,1}(\tau_1, \tau_2)|^2 d\tau_1 d\tau_2$. The success probability of shaping, denoted as β , can be expressed as

$$\beta = P_{1,1} \left| \int_{t_{\text{dec}}-t_R/2}^{t_{\text{dec}}+t_R/2} d\tau_1 \int d\tau_2 |F_{m,2-m}(\tau_1, \tau_2)|^2 \right|. \quad (\text{D2})$$

Therefore, if the resolved time t_R approaches to 0, the corresponding success probability approaches to 0 too. In the case of limited detection resolution, the fidelity could be re-expressed as

$$F_{\text{shaping}} = \left| \int_{t_{\text{dec}}-t_R/2}^{t_{\text{dec}}+t_R/2} d\tau_1 \int d\tau_2 \frac{F_{1,1}(\tau_1, \tau_2)}{\sqrt{\text{nor}}} \frac{f_{\text{Target}}^*(\tau_2)}{\sqrt{t_R}} \right|^2. \quad (\text{D3})$$

Here $f_{\text{Target}}(\tau)$ denotes the target temporal shape which could be ED sine or Gaussian shape. The effect of limited resolved time t_R on the shaping fidelity F_{shaping} and success probability β for ED shape and Gaussian shape is shown in Fig. 5. With the increase of the resolved time t_R , the success probability gradually increases from zero, while the fidelity decreases from its maximum value.

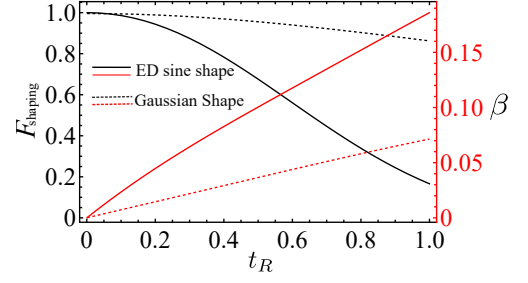


FIG. 5. Effect of limited detection resolution t_R on the shaping fidelity (black lines) and success probability (red lines) for generating photon with ED shape (solid curves) and Gaussian shape (dashed curves).

-
- [1] C. K. Hong, Z. Y. Ou, and L. Mandel, *Phys. Rev. Lett.* **59**, 2044 (1987).
- [2] E. Knill, R. Laflamme, and G. J. Milburn, *Nature* **409**, 46 (2001).
- [3] P. Kok, W. J. Munro, K. Nemoto, T. C. Ralph, J. P. Dowling, and G. J. Milburn, *Rev. Mod. Phys.* **79**, 135 (2007).
- [4] G. Vittorini, D. Hucul, I. V. Inlek, C. Crocker, and C. Monroe, *Phys. Rev. A* **90**, 040302(R) (2014).
- [5] S. Laibacher and V. Tamma, *Phys. Rev. A* **98**, 053829 (2018).
- [6] T.-M. Zhao, H. Zhang, J. Yang, Z.-R. Sang, X. Jiang, X.-H. Bao, and J.-W. Pan, *Phys. Rev. Lett.* **112**, 103602 (2014).
- [7] C. Dangel, J. Schmitt, A. J. Bennett, K. Müller, and J. J. Finley, *Phys. Rev. Appl.* **18**, 054005 (2022).
- [8] T. Legero, T. Wilk, A. Kuhn, and G. Rempe, *Appl. Phys. B* **77**, 797 (2003).
- [9] V. Tamma and S. Laibacher, *Phys. Rev. Lett.* **114**, 243601 (2015).
- [10] T. Legero, T. Wilk, M. Hennrich, G. Rempe, and A. Kuhn, *Phys. Rev. Lett.* **93**, 070503 (2004).
- [11] X.-J. Wang, B. Jing, P.-F. Sun, C.-W. Yang, Y. Yu, V. Tamma, X.-H. Bao, and J.-W. Pan, *Phys. Rev. Lett.* **121**, 080501 (2018).
- [12] E. Rephaeli, J.-T. Shen, and S. Fan, *Phys. Rev. A* **82**, 033804 (2010).
- [13] E. Rephaeli and S. Fan, *Phys. Rev. Lett.* **108**, 143602 (2012).
- [14] M. Cotrufo and A. Alù, *Optica* **6**, 799 (2019).
- [15] Z. Liao, H. Nha, and M. S. Zubairy, *Phys. Rev. A* **94**, 053842 (2016).
- [16] J. I. Cirac, P. Zoller, H. J. Kimble, and H. Mabuchi, *Phys. Rev. Lett.* **78**, 3221 (1997).
- [17] M. Heuck, K. Jacobs, and D. R. Englund, *Phys. Rev. Lett.* **124**, 160501 (2020).

- [18] M. Li, Y.-L. Zhang, H. X. Tang, C.-H. Dong, G.-C. Guo, and C.-L. Zou, *Phys. Rev. Appl.* **13**, 044013 (2020).
- [19] Z. Tian, P. Zhang, and X.-W. Chen, *Phys. Rev. Appl.* **15**, 054043 (2021).
- [20] M. F. Yanik and S. Fan, *Phys. Rev. Lett.* **93**, 173903 (2004).
- [21] L. Yuan, M. Xiao, and S. Fan, *Phys. Rev. B* **94**, 140303(R) (2016).
- [22] S.-Y. Baek, O. Kwon, and Y.-H. Kim, *Phys. Rev. A* **77**, 013829 (2008).
- [23] V. Averchenko, D. Sych, G. Schunk, U. Vogl, C. Marquardt, and G. Leuchs, *Phys. Rev. A* **96**, 043822 (2017).
- [24] D. Sych, V. Averchenko, and G. Leuchs, *Phys. Rev. A* **96**, 053847 (2017).
- [25] K. J. Blow, R. Loudon, S. J. D. Phoenix, and T. J. Shepherd, *Phys. Rev. A* **42**, 4102 (1990).
- [26] V. V. Orre, E. A. Goldschmidt, A. Deshpande, A. V. Gorshkov, V. Tamma, M. Hafezi, and S. Mittal, *Phys. Rev. Lett.* **123**, 123603 (2019).
- [27] T. Gerrits, F. Marsili, V. B. Verma, L. K. Shalm, M. Shaw, R. P. Mirin, and S. W. Nam, *Phys. Rev. A* **91**, 013830 (2015).
- [28] M. Li, Y.-L. Zhang, H. X. Tang, C.-H. Dong, G.-C. Guo, and C.-L. Zou, *Phys. Rev. Appl.* **13**, 044013 (2020).
- [29] C. K. Law, I. A. Walmsley, and J. H. Eberly, *Phys. Rev. Lett.* **84**, 5304 (2000).